AIAA 81-0149R

Experimental Forces and Moments on Cone-Derived Waveriders for $M_\infty = 3$ to 5

M.L. Rasmussen* and M.C. Jischke†
University of Oklahoma, Norman, Oklahoma
and
D.C. Daniel‡
Air Force Armament Laboratory, Eglin AFB, Florida

Six components of force and moment data are presented for two cone-derived waverider lifting body configurations in the Mach number range 3 to 5 and the unit Reynolds number range 1 to 2 M/ft. Angle of attack and sideslip angle were varied in the range ±20 deg. As a basis for comparison, data are also presented for an elliptic cone with a 1.87 major-minor axis ratio. Schlieren data for the waverider shock wave positions are also presented. Maximum lift-to-drag ratios of the waveriders are found to be 2.5 times greater than for the elliptic cone. Normal force and rolling moment coefficients, along with the lift-to-drag ratios, are found to decrease for the waveriders as M_∞ increases.

Nomenclature

A_b = base area
C_N = normal force coefficient, $-F_z/qA_b$
C_A = axial force coefficient, $-F_x/qA_b$
C_y = side force coefficient, F_y/qA_b
C_ℓ = rolling moment coefficient, M_x/qA_bL
C_m = pitching moment coefficient, M_y/qA_bL
C_n = yawing moment coefficient, M_z/qA_bL
C_L = lift coefficient, lift$/qA_b$
C_D = drag coefficient, drag$/qA_b$
C_p = pressure coefficient, $(p-p_\infty)/q$
K_δ = hypersonic similarity parameter, $M_\infty\delta$
L = length of body
q = $\frac{1}{2}\rho_\infty V_\infty^2$
M_∞ = freestream Mach number
α = angle of attack
β = angle of sideslip
β_0 = shock semivertex angle for basic cone
δ = semivertex angle of basic cone
ϵ = Fourier expansion cross-section eccentricity
Λ = dihedral angle
σ = β_0/δ, Eq. (8)
θ = polar angle
ϕ = azimuthal angle

Introduction

EXTREME performance and maneuverability requirements for future missiles operating in the high-supersonic, low-hypersonic Mach number range will require high-lift, low-drag configurations with good control effectiveness. Noncircular airframe configurations that efficiently integrate volumetric storage, lifting capability, and propulsion components, such that aerodynamic heating and radar cross section are minimized and lift-to-drag ratios are maximized, will be required. Discussions of such requirements are given by Giragosian,[1] Fleeman,[2] and Nielsen.[3]

A comprehensive research program is underway that addresses many of these requirements and is directed toward the study of lifting body configurations operating at the high Mach numbers of interest. The theoretical analysis is based on small perturbations of axisymmetric flows past circular cones, the perturbations stemming from small angles of attack and small eccentricity of the cone cross section. By this means accurate approximate analytical results are obtained for shock shapes and the shock-layer structure. Since any stream surface can be utilized as a solid surface in an inviscid flow, lifting body configurations are constructed when freestream upper surfaces are selected to complement the lower conical flow stream surfaces. These resulting aerodynamic shapes are called cone-derived waveriders because they appear to ride on a conical shock wave attached beneath them. The generation of certain specific shapes and the properties of their shock-layer structures are discussed by Rasmussen.[4] The generalization of this analysis for arbitrary small conical perturbations of a basic axisymmetric conical flow is given by Jischke.[5] Nearly all previous work regarding waveriders deals with caret shapes or shapes derived from axisymmetric flow. General considerations relating to the aerodynamic performance of waverider configurations are discussed by Küchemann.[6]

Surface pressure measurements for a type of waverider derived from axisymmetric conical flowfields have been reported by Pike.[7] Although these waveriders are similar to those considered here, the bodies themselves are not conical, even though their flowfields are. No direct force and moment measurements were taken.

In this paper extensive experimental results are presented for the forces and moments on two fundamental cone-derived waveriders, which are themselves conical. These two waverider configurations were selected from examples illustrated and discussed by Rasmussen.[4] To provide a basis for comparison, experiments were also conducted on two other basic configurations: an elliptic cone with a major-minor axis ratio of 1.87, and this same elliptic cone with thin delta winglets attached on the major-axis plane. Six components of force and moment data were obtained for a variation of ±20 deg in angle of attack and sideslip over a Mach number range of 3 to 5. Schlieren and surface oil flow visual data were also obtained.

Description of Models

Sketches of model configurations that were tested are given in Figs. 1a-c. All the models were constructed of stainless steel

Presented as Paper 81-0149 at the AIAA 19th Aerospace Sciences Meeting, St. Louis, Mo., Jan. 12-15, 1981; submitted Feb. 27, 1981; revision received April 8, 1982.

*Professor, Aerospace, Mechanical, and Nuclear Engineering. Associate Fellow AIAA.
†Dean, School of Engineering. Associate Fellow AIAA.
‡Research Manager. Associate Fellow AIAA.

and had the same length, $L = 60$ cm $\simeq 23.62$ in., measured along the basic cone axis from which they were derived. The other dimensions are indicated in Fig. 1 and given in inches in Table 1, along with the base area, A_b, in square inches. The position of the fixed-body (or sting) coordinate system, to which the six force and moment components are referred, is also shown. The jagged curves in Fig. 1 indicate the theoretical position of the shock wave at the design condition $M_\infty = 4$.

The model shown in Fig. 1a was derived from the flow past a circular cone at angle of attack, as explained in Ref. 4. It is referred to as the circular cone waverider. The flow in the shock layer is the same as the flow on the leeward side of an inclined circular cone. The shape of the curved surface, which is a conical stream surface in the inclined cone flow, has been approximated by the method of analysis of Ref. 4, and is given in spherical coordinates by

$$\frac{\theta}{\delta} = 1 + 0.34\left[\tan\left(\frac{\pi}{2} - \frac{\phi}{2}\right)\right]^{12.5} \tag{1}$$

where θ is the polar angle measured from the basic cone axis (parallel to the x axis but passing through the vertex), and ϕ is the azimuthal angle measured around the basic cone axis such that $\phi = \pi$ in the z direction. The semivertex angle for the basic cone is denoted by δ, which for this model is $\delta = 18.62$ deg. The angle of attack defining this waverider configuration was selected as $\alpha/\delta = 0.2$, or $\alpha = 3.72$ deg, which determines the angle between the basic cone axis and the symmetry ray of the upper surface.

The model shown in Fig. 1b was derived from the flow past an elliptic cone at zero angle of attack and is referred to as the elliptic cone waverider. The shape of the curved surface, which is a conical stream surface for the elliptic cone flow, is given approximately by

$$\frac{\theta}{\delta} = 1 - 0.1\cos 2\phi + (0.39 + 0.1\cos 2\phi)\left[\frac{\tan(\pi - \phi)}{2.75}\right]^{7.69} \tag{2}$$

Table 1 Model dimensions, in.

	L	W	T	R	A_b, in.^{2}
Circular cone waverider	23.62	21.98	7.96	4.46	103.60
Elliptic cone waverider	23.62	21.50	7.11	4.62	75.83
Elliptic cone	23.62	22.68	12.16	6.08	216.60

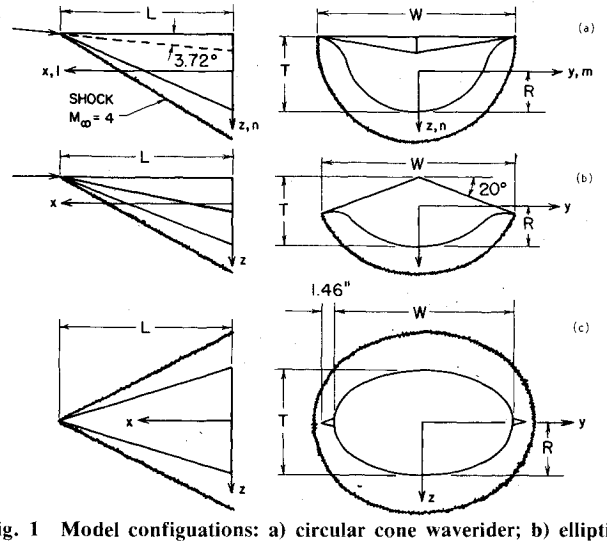

Fig. 1 Model configuations: a) circular cone waverider; b) elliptic cone waverider; c) elliptic cone with winglets.

The basic cone angle for this model was also selected as $\delta = 18.62$ deg. The eccentricity, as defined by the Fourier series representation of Ref. 4, was selected such that $\epsilon/\delta = 0.1$.

The design Mach number for these waverider models is $M_\infty = 4$. Thus the pertinent hypersonic similarity parameter is $K_\delta \equiv M_\infty \delta = 1.3$. This value of K_δ was used to determine the numerical factors in Eqs. (1) and (2). According to Ref. 4, the circular cone waverider, model 1a, is said to have a positive dihedral, and the elliptic cone waverider, model 1b, is said to have a negative dihedral. A photograph giving the side view of the elliptic cone waverider is shown in Fig. 2.

For the on-design condition, the theoretical shock shape for model 1a is

$$\theta_s/\delta = 1.34 - 0.04\cos\phi \tag{3}$$

and for model 1b the shock shape is

$$\theta_s/\delta = 1.34 - 0.06\cos 2\phi \tag{4}$$

These shocks are attached to the waverider lips at $\phi = 90$ deg for model 1a and at $\phi = 110$ deg for model 1b.

Figure 1c shows the elliptic cone model with winglets attached on the plane of the major axis. The equation for the elliptic cone in spherical coordinates is

$$\tan\theta = \frac{\tan\theta_m}{\sqrt{1 + e\cos 2\phi}} \tag{5}$$

with $\theta_m = 17.79$ deg and $e = 0.5534$. These values correspond to a major-minor axis ratio of 1.87. According to the perturbation analysis of Ref. 4, the corresponding basic cone angle is 18.68 deg, which is nearly the same as for the two waverider models. The pertinent hypersonic similarity parameter is thus about $K_\delta = 1.3$ for $M_\infty = 4$. The perturbation analysis of Ref. 4 yields an eccentricity factor of $\epsilon/\delta = 0.478$. This elliptic cone is thus much more eccentric than the elliptic cone from which waverider 1b was derived. The delta winglets that could be attached on the major-axis plane were wedge-shaped with a 5 deg included angle at the sharp leading edge, and they were 1.47 in. wide at the base. The winglets were designed to extend out to the shock position that would exist at $M_\infty = 4$ without the winglets. Tests were run with and without the winglets attached.

Experimental Conditions

The tests were run in wind tunnel A of the von Kármán facility at the USAF Arnold Engineering Development Center. Tunnel A is a continuous-flow, closed-circuit, variable-density wind tunnel with an automatically driven flexible plate-type nozzle and 40×40 in. test section. The tunnel is equipped with a model injection system that allows removal of the model from the test section while the tunnel remains in operation. A complete description of the tunnel and airflow calibration information may be found in Ref. 8.

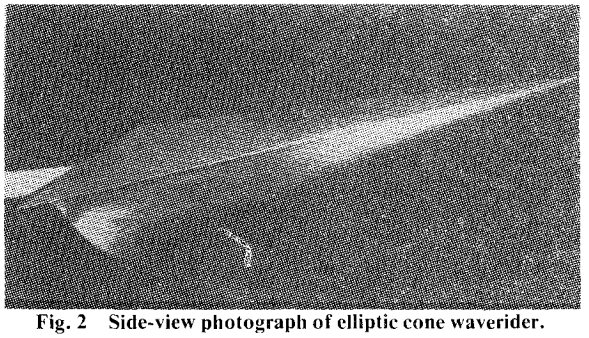

Fig. 2 Side-view photograph of elliptic cone waverider.

The experiments were conducted at Mach numbers 3.0, 3.5, 4.0, 4.5, and 5.0. On-design conditions for the waveriders were at $M_\infty = 4.0$ and $\alpha = -3.72$ deg for the circular cone waverider and $\alpha = 0$ for the elliptic cone waverider, both with zero sideslip. All other conditions were off-design conditions. Six components of force and moment data were recorded for angles of attack and sideslip in the range ± 20 deg. Schlieren data were recorded during these tests from which shock wave positions could be measured and flow patterns observed. Oil flow tests were also conducted.

The nominal unit Reynolds number for the tests was 2 million per ft (M/ft). Tests were also conducted at unit Reynolds number of 1 M/ft on the circular cone waverider at Mach numbers 3.0, 3.5, 4.0, and 4.5. Because there was no noticeable effect of unit Reynolds number in this range, all the remaining tests were conducted at the nominal unit Reynolds number of 2 M/ft. A complete summary of the test conditions is given in Ref. 9.

Forces and Moments

The data for the forces and moments will be presented in three comparative groups. First, the six components of force and moment coefficients will be presented in body-fixed coordinates for $M_\infty = 4$, comparing the four aerodynamic configurations. The second group will compare the corresponding lift and drag coefficients of the four configurations at $M_\infty = 4$. The third group will concern the effects of variation in freestream Mach number. All forces and moments are for the forebody contribution.

Approximating Formulas

The discussion of these results is facilitated by the use of simple approximate formulas for the normal force and axial force coefficients of an idealized conical waverider at on-design conditions. Consider axisymmetric hypersonic flow past a slender circular cone of semivertex angle δ with a conical shock of semivertex angle β_0. Any plane passing through the cone axis is a stream surface in the shock layer. Choose a pair of axial planes with a dihedral angle Λ measured from a horizontal axial plane. Select the portion of these planes between the body and shock as infinitesimal-thickness delta wings, and construct the idealized conical waverider shown in Fig. 3. If the pressure in the shock layer is approximated as a constant evaluated at the cone surface conditions, then the normal force and axial force coefficients for the on-design conditions are

$$C_N \simeq \left(\frac{C_p}{\delta^2}\right)\frac{2\delta}{\pi}\,\frac{\sigma\cos\Lambda}{1+2\Lambda/\pi} \tag{6}$$

$$C_A \simeq \left(\frac{C_p}{\delta^2}\right)\delta^2 \tag{7}$$

where[4]

$$\sigma \equiv \frac{\beta_0}{\delta} = \left[\frac{\gamma+1}{2} + \frac{1}{K_\delta^2}\right]^{1/2} \tag{8}$$

$$\frac{C_p}{\delta^2} = 1 + \frac{\sigma^2 \ell n \sigma^2}{\sigma^2 - 1} \tag{9}$$

and $K_\delta \equiv M_\infty \delta$ is the hypersonic similarity parameter. For the present circular cone waverider, $\Lambda = 0$, whereas for the elliptic cone waverider, $\Lambda = -20$ deg. For the present on-design conditions, $K_\delta = 1.3$, $\sigma = 1.34$, $C_{p_0}/\sigma^2 \to \delta^2 = 2.32$, and $\delta = 18.6$ deg. The approximate formulas (6) and (7) may be used to extend the present results to other conditions and configurations.

Body-Fixed Force Components

Figures 4 and 5 show the normal force and axial force coefficients for the different models as a function of angle of attack at $M_\infty = 4$ at unit Reynolds number of 2 M/ft and at zero sideslip angle. The force and moment coefficients were normalized with the individual base areas of the models, and this should be kept in mind when comparing the actual forces on the models. The elliptic cone waverider produces the largest normal force coefficient at $\alpha = 20$ deg and also the largest negative value at $\alpha = -20$ deg. The C_N vs α curve is nearly linear over this angle-of-attack range and also has the largest slope, $C_{N_\alpha} \simeq 5.63$/rad. The normal force coefficient for the circular cone waverider is nearly bilinear, that is, the slope C_{N_α} has one constant value for positive α and a different constant value for negative α. Even when the larger reference base area of the circular cone waverider is taken into account, the elliptic cone waverider produces a larger normal force than the circular cone waverider for on-design conditions and positive angles of attack. Compared to the results in Fig. 4, formula (6) gives a slightly smaller value for C_N for the on-design elliptic cone waverider ($\alpha = 0$) and a slightly larger value for the on-design circular cone waverider ($\alpha = -3.72$ deg).

As a basis for comparison, Fig. 3 also shows the normal force coefficients for the elliptic cone. When the cross flow is perpendicular to the *minor* axis of the elliptic cone, the orientation is referred to as the *transverse condition* (trans). Without this restriction the cross flow is understood to be perpendicular to the major axis. The slope of the normal force curve for the nontransverse condition is approximately 2.25 times greater than the transverse condition. The winglets attached to the elliptic cone produce about a 14% increase in

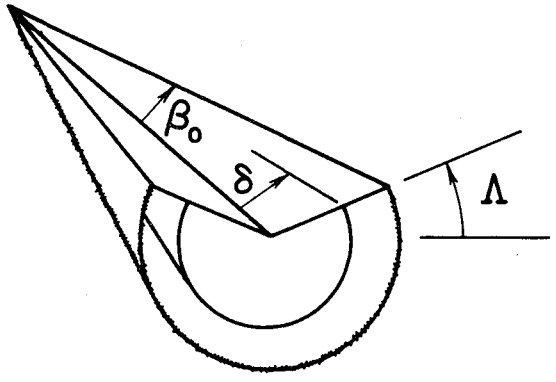

Fig. 3 Idealized conical waverider.

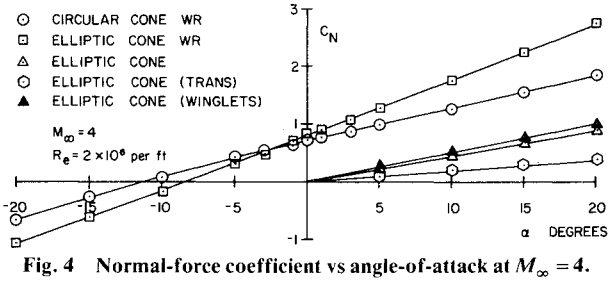

Fig. 4 Normal-force coefficient vs angle-of-attack at $M_\infty = 4$.

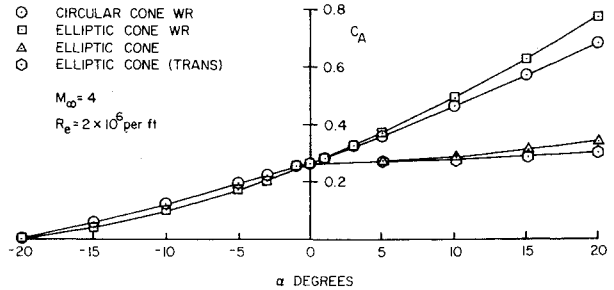

Fig. 5 Axial-force coefficient vs angle-of-attack at $M_\infty = 4$.

the slope of the normal force curve over the elliptic cone without winglets. The effects of the winglets are found to be small compared to the differences between the other configurations. At $\alpha = 20$ deg the C_N for the elliptic cone waverider is 3.15 times greater than for the elliptic cone, and 1.49 times greater than for the circular cone waverider. The elliptic cone waverider produces the largest actual normal force. The angle of zero normal force occurs at $\alpha = -8.4$ deg for the elliptic cone waverider and at $\alpha = -11.2$ deg for the circular cone waverider.

The axial force coefficients for the two waveriders and the elliptic cone are shown in Fig. 5. The base drag has been subtracted from the force contribution on the models. The elliptic cone waverider has the largest values of C_A for positive angles of attack. At $\alpha = 0$, all the configurations have about the same value of $C_A \simeq 0.266$. This is consistent with formula (7) since K_δ and δ are nearly the same for all. The theoretical value of C_A from formula (7), however, is 8% lower than the experimental value. The axial force on the waveriders vanishes when $\alpha \simeq -20$ deg. The effect of the winglets on C_A for the elliptic cone is very small and thus is not shown.

Figure 6 shows the side force coefficients for $M_\infty = 4$ as a function of sideslip angle, β, for $\alpha = 0$. (A negative sideslip angle corresponds to a positive rotation about the z axis.) Because the models are all symmetric about the x-z plane, only values for negative β are shown. The data for the circular cone waverider illustrate the negligible change when unit Reynolds number is varied between 1 and 2 M/ft. The side force coefficients are nearly linear with β. The side force coefficients for the circular cone waverider are the largest, and the smallest for the elliptic cone waverider, with transverse flow past the elliptic cone in between. The actual side force for the transverse elliptic cone is really the largest of the three shown since it has a reference base area 2.09 times greater than the circular cone waverider.

Body-Fixed Moment Coefficients

Figures 7-9 show the moment coefficients C_ℓ, C_m, and C_n for the moments about the x, y, and z axes for $M_\infty = 4$. Figure 7 shows the rolling moment coefficient C_ℓ as a function of sideslip angle (with $\alpha = 0$). The circular cone waverider illustrates negligible change with unit Reynolds numbers in the range 1 to 2 M/ft. The rolling moments are nearly linear with β, with C_ℓ for the circular cone waverider being about 3.1 times greater than that of the elliptic cone waverider. The rolling moments for cross flows perpendicular to the major or minor axes of the elliptic cone are zero owing to symmetry.

Figure 8 shows the pitching moment coefficients as a function of angle of attack (with $\beta = 0$), reckoned about the y axes located at the bases of the models. The pitching moment curves are nearly linear and are similar in appearance to the normal force curves in Fig. 4. The ratios C_m/C_N, for given values of α, are nearly constant (except for the waveriders in the immediate vicinity of $C_N = 0$). Except very near $C_N = 0$, the average value of C_m/C_N over the range $\alpha = \pm 20$ deg is $C_m/C_N \simeq 0.32$ for the elliptic cone waverider, and $C_m/C_N \simeq 0.33$ for the circular cone waverider. The corresponding values for the elliptic cone are $C_m/C_N \simeq 0.29$ and $C_m/C_N \simeq 0.18$ for the transverse orientation. As a basis for comparison, the ratio for the basic cone is $C_m/C_N =$

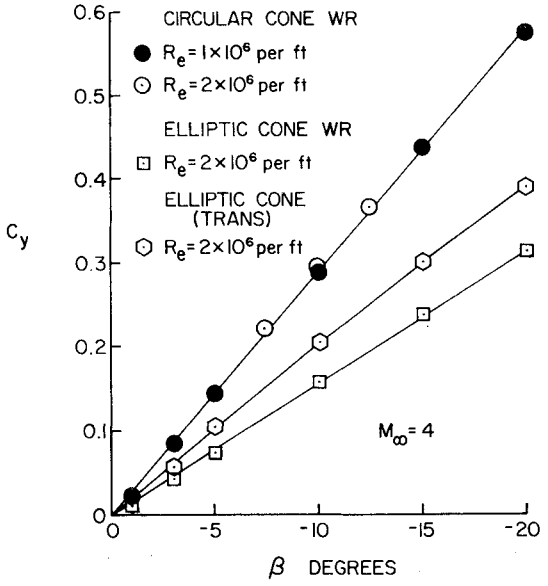

Fig. 6 Side-force coefficient vs sideslip angle at $M_\infty = 4$.

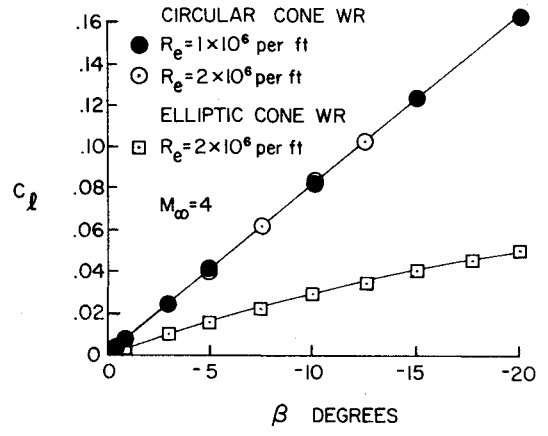

Fig. 7 Rolling moment coefficient vs sideslip angle at $M_\infty = 4$.

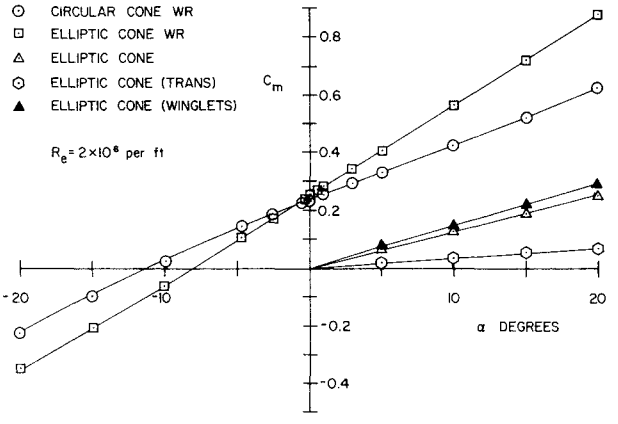

Fig. 8 Pitching moment coefficient vs angle-of-attack at $M_\infty = 4$.

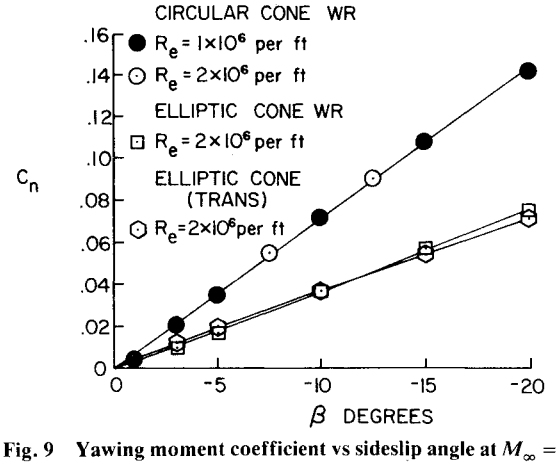

Fig. 9 Yawing moment coefficient vs sideslip angle at $M_\infty = 4$.

$1-(\frac{2}{3}\sec^2\delta \simeq 0.26$, which for the axisymmetric basic cone is the center of pressure measured as a percent of L from the base.

The yaw moment coefficients, corresponding to moments about the z axis, are shown in Fig. 9 as a function of sideslip angles (with $\alpha=0$). The curves for the waveriders are nearly linear. The ratios C_n/C_y, for fixed β, are nearly constant over the range of variation of β. The value of C_n/C_y for the elliptic cone waverider is about $C_n/C_y \simeq 0.24$, and the corresponding value for the circular cone waverider is $C_n/C_y \simeq 0.25$. The curve for the elliptic cone waverider is not as linear as for the elliptic cone waverider, starting above the elliptic cone waverider curve for small β and ending slightly below it for large β; the average value of C_n/C_y is about 0.18.

Lift and Drag Coefficients

Figures 10-12 show the lift coefficients, the drag coefficients, and the L/D ratios as functions of angle of attack. The curves for C_L in Fig. 10 are similar to the corresponding curves for C_N, but are noticeably nonlinear as should be expected from the geometrically related definitions. The elliptic cone waverider shows the greatest lifting ability of the four models. The values of $C_L \simeq C_N$ at on-design conditions

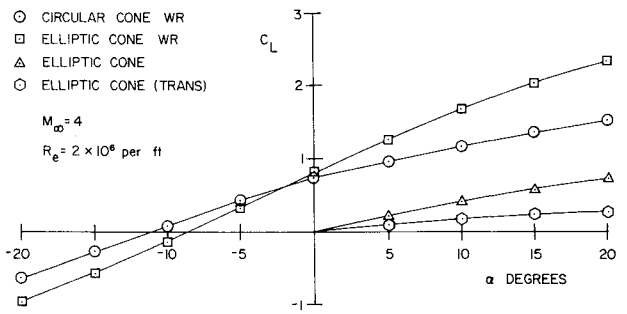

Fig. 10 Lift coefficient vs angle-of-atack at $M_\infty = 4$.

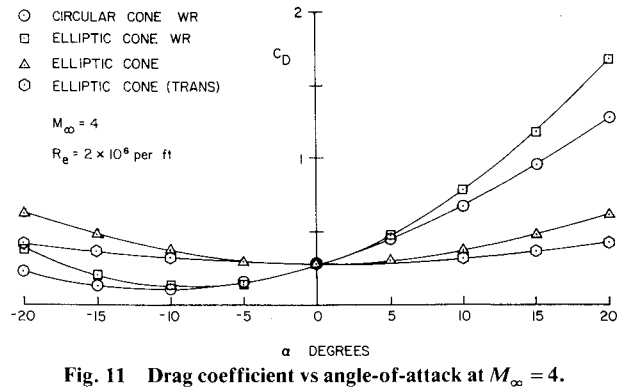

Fig. 11 Drag coefficient vs angle-of-attack at $M_\infty = 4$.

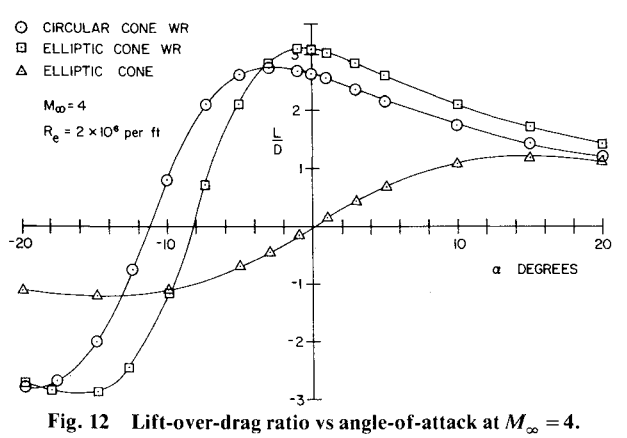

Fig. 12 Lift-over-drag ratio vs angle-of-attack at $M_\infty = 4$.

are approximated by formula (6) for the waveriders. The drag coefficients shown in Fig. 11 are decidedly nonlinear, varying approximately as α^2 about the angle of zero lift, which is -8.6 deg for the elliptic cone waverider and -11.2 deg for the circular cone waverider. The drag coefficients are approximately the same for all the models at $\alpha=0$, in accordance with Eq. (7). At the design conditions, the circular cone waverider drag coefficient is less than the elliptic cone waverider drag coefficient, but the actual drag values are nearly the same when the differences in base areas are taken into account. The drag force for the on-design waveriders is much less than the elliptic cone generating the same lift.

Figure 12 shows the L/D ratios, which are an important measure of aerodynamic efficiency. The L/D ratios are independent of the base areas of reference for the different models. The waverider models achieve their maximum value of L/D at their design orientations, with the elliptic cone waverider having the largest value. The maximum value of L/D for the elliptic cone waverider (at $\alpha=0$) is 2.5 times greater than the maximum value of L/D for the elliptic cone (at $\alpha=15$ deg). The waverider models also have negative values of L/D which occur at negative angles of attack; the minimum L/D values have nearly the same absolute values as the on-design conditions. The ratio of Eqs. (6) and (7) gives a good approximation for the maximum L/D for the waveriders:

$$\left(\frac{L}{D}\right)_{\max} \simeq \frac{2}{\pi\delta}\,\frac{\sigma\cos\Lambda}{1+2\Lambda/\pi} \tag{10}$$

Formula (10) simply shows how δ, σ, and Λ affect the maximum L/D ratios for the waveriders on design. Smaller values of δ, that is, more slender bodies, increase the value of L/D, and negative dihedral tends also to increase L/D.

Mach Number Effects

Figures 13-15 illustrate the effects of Mach number changes from 3 to 5 for the waveriders. The Mach number effects for the elliptic cones were much smaller, and thus only their results for $M_\infty=4$ are shown for comparison purposes. For example, for the elliptic cone at $\alpha=20$ deg, C_N decreased from 0.90 to 0.85 as M_∞ increased from 3 to 5, but the maximum value of L/D did not vary significantly from 1.2. The largest effects of changes on Mach number for the waverider configurations were on the normal force coefficients and the rolling moment coefficients. The variation of C_N with Mach number is shown in Fig. 13 for the circular cone waverider and in Fig. 14 for the elliptic cone waverider. As M_∞ increases from 3 to 5, the absolute value of C_N decreases. The waveriders have a higher C_N for Mach numbers smaller than the design value. The axial force coefficients (not shown) show much smaller variations with Mach number. For the elliptic cone waverider at $\alpha=0$, L/D decreased from 3.22 to 2.90 as M_∞ increased from 3 to 5. Figure 15 shows the effect of Mach number changes on the rolling moment coefficients C_ℓ for the waveriders. Increasing the Mach number causes the rolling moment to decrease.

Shock Wave Configurations

Some of the features of the flowfield and shock wave configurations were determined from schlieren photography. Schlieren photographs were taken at selected angles of attack and sideslip angles during the force and moment measurements. In addition, photographs were taken at 10 deg intervals in roll about the x axis. Examples of these schlieren data are shown in Fig. 16 for the elliptic cone waverider at $\alpha=0$; the roll angles are for 0 and 90 deg and for Mach numbers of 3, 3.5, 4, 4.5, and 5. The first column of these photographs shows the side view of the waverider (zero roll). The lower part of the shock wave can be seen and measured. For the upper part of the flow, no shock disturbance can be seen. This is in accordance with the on-design condition of the

waverider at $M_\infty = 4$, since the flow is aligned with the upper surface, and the entire flow disturbance is meant to be contained in the attached shock layer beneath the waverider. The second column of Fig. 16 shows the planform configuration at 90-deg roll. For the off-design conditions $M_\infty = 3$ and 3.5 in the first two photographs, the shock wave is seen to be detached from the lip. Since there is no upper shock wave seen in the corresponding side views, this detached conical shock degenerates to a Mach wave at the upper ray in the symmetry plane. At the upper off-design conditions $M_\infty = 4.5$ and 5, the lower planform views in the second column show the shock wave to be attached to the waverider.

The data from the schlieren photograps in Fig. 16 can be used to infer the shock shapes in the y-z plane as shown in Fig. 17. The attached shock beneath the waverider is the theoretical on-design shock shape for $M_\infty = 4$ computed from Eq. (4). The actual shock angle at the lower ray for $M_\infty = 4$ measured from the photograph is slightly greater than the theoretical result; in fact, the actual shock at $M_\infty = 4$ appears very slightly detached from the body. For the higher Mach numbers 4.5 and 5, the shock waves are attached beneath the body, and the lower ray comes closer to the body as M_∞ increases. For the lower Mach numbers 3 and 3.5 the conical shock wave is detached (except at the vertex), and the faired shock curves through the data points in Fig. 17 are inferred. The data points for the top ray ($\phi = 0$) are the theoretical Mach angles extending from the vertex, since no disturbance was observed from the schlieren photographs. The dashed curve above the waverider is the theoretical Mach surface for the on-design condition $M_\infty = 4$. Similar Mach surfaces also exist for $M_\infty = 4.5$ and 5, but they are not shown. The shock waves above the waverider approach the Mach surface as M_∞ approaches 4 from below.

Similar results were found for the circular cone waverider. The shock was found to be very slightly detached from the lip at $M_\infty = 4$, and attached as for the elliptic cone waverider for the higher Mach numbers. From the schlieren photographs of the elliptic cone at $M_\infty = 4$ and $\alpha = 0$, it was determined that the shock stands off from the base of the body 2.27 in. from the major axis and 4.40 in. from the minor axis, as indicated in Fig. 1c.

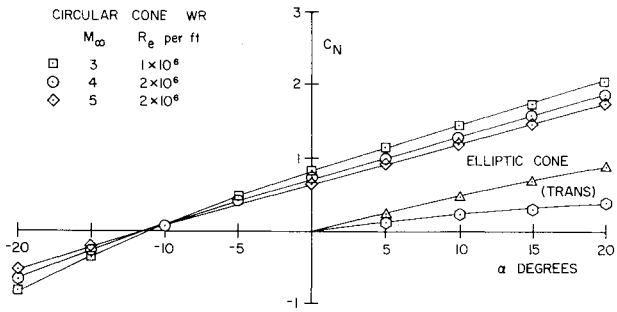

Fig. 13 Mach number variation of C_N vs α for circular-cone waverider.

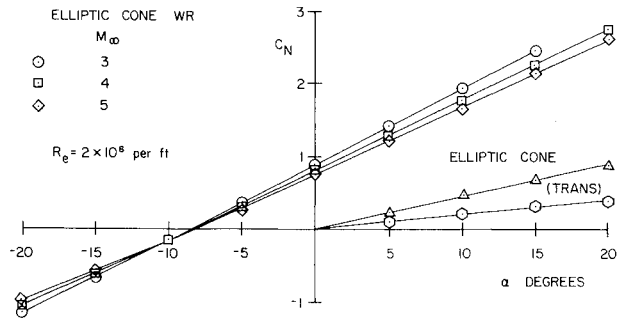

Fig. 14 Mach number variation of C_N vs α for elliptic-cone waverider.

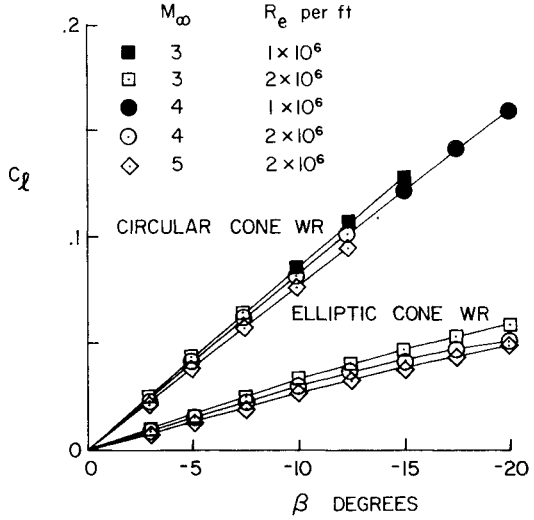

Fig. 15 Mach number variation of C_ℓ vs β for waveriders.

Oil Flow Results

Oil flow visualization data were obtained on each model configuration at $M_\infty = 3.5$, 4.0, and 4.5 and at a unit

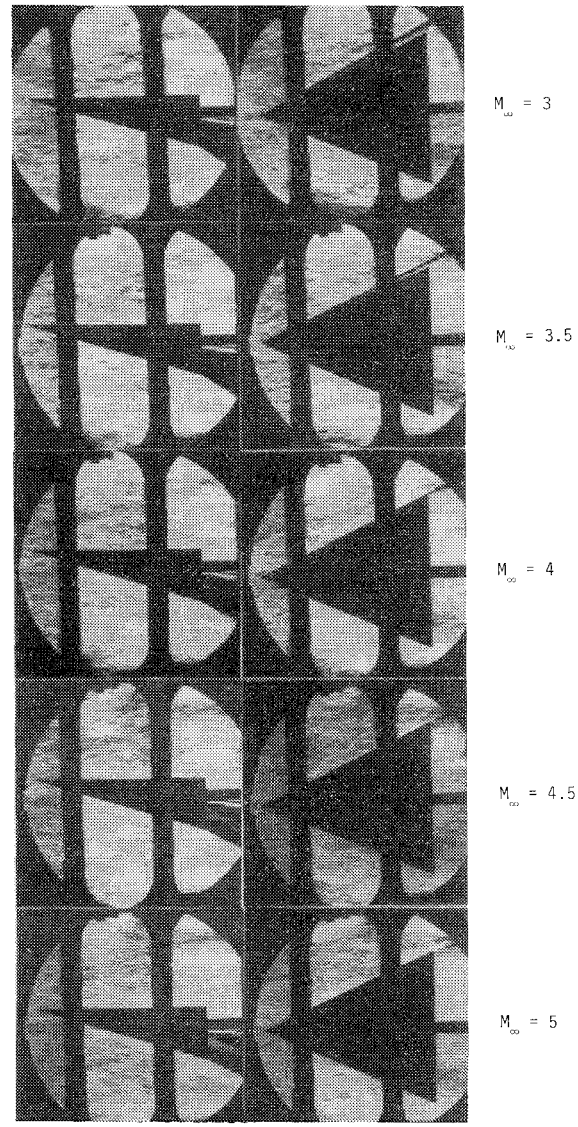

Fig. 16 Schlieren photographs of side views and plan views of elliptic-cone waverider.

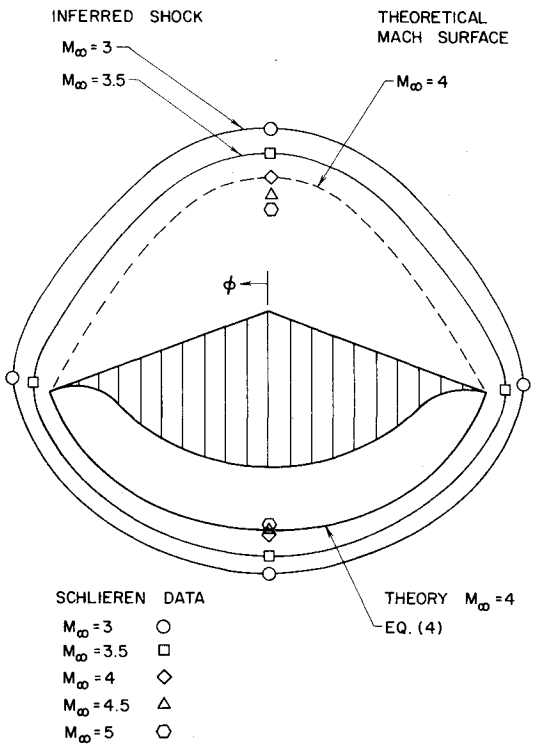

Fig. 17 Cross-section shock shapes for elliptic-cone waverider.

Reynolds number of 2 M/ft. The top and bottom surfaces of the models were photographed simultaneously at angles of attack of -10, -3.7, 10, and 17.5 deg for zero sideslip and at a sideslip angle of -10 deg for zero angle of attack. From these photographs the boundary layer always appeared laminar, and no transition to turbulence was observed. A kind of cleansing of the oil from the surface near sharp corners occurred, and distinctive patterns of oil flow occurred on the curved surfaces near the nose, apparently owing to viscous shear effects.

Discussions and Conclusions

A comprehensive set of data for the forces and moments on two cone-derived waveriders has been presented together with a corresponding comparative set for an elliptic cone. The conical waverider models are taken from a fundamental generic class of lifting bodies. The on-design condition for these bodies is accurately described by the perturbation theory of Ref. 4. The data substantiate the accuracy of the theory for the on-design conditions and show the deviations resulting from changes in both orientation and Mach number. The waverides produce significantly larger lift forces than the comparative elliptic cone. The winglets on the elliptic cone, which were meant to fashion a pseudowaverider configuration, produced only modest improvements in lift over the elliptic cone without the winglets. The L/D ratio, representing a factor of aerodynamic efficiency, was 2.5 times greater for the on-design elliptic cone waverider than for the maximum L/D for the elliptic cone. The forces and moments on the waveriders decreased as the Mach number increased from 3 to 5. The schlieren data together with the surface oil flow results provide additional information that the flows were always conical and clean, without strong secondary shocks or interruptions, over the entire range of testing conditions. These tests taken with the supporting theoretical background make the cone-derived waveriders very attractive and viable contenders for future hypersonic missile and aircraft configurations.

Acknowledgments

This work was sponsored by the Air Force Armament Laboratory under Contract F08635-79-C-0017. The authors gratefully acknowledge the graphical aid of Paul R. Mackin and Scott R. Swinsick in the preparation of this paper.

References

[1] Giragosian, P.A., "Critical Aerodynamic Technology Issues in Air-to-Air Missile Design," AIAA Paper 79-0089, Jan. 1979.

[2] Fleeman, E.L., "Aeromechanics Technologies for Tactical and Strategic Guided Missiles," presented at the AGARD FMP Meeting on Missile Systems Flight Mechanics, London, May 1979.

[3] Nielsen, J.N., "Missile Aerodynamics—Past, Present, Future," AIAA Paper 79-1819 (Wright Brothers Lectureship in Aeronautics), Aug. 1979.

[4] Rasmussen, M.L., "Waverider Configurations Derived from Incined Circular and Elliptic Cones," *Journal of Spacecraft and Rockets,* Vol. 17, Nov.-Dec. 1980, pp. 537-545.

[5] Jischke, M.C., "Supersonic Flow Past Conical Bodies with Nearly Circular Cross Sections," *AIAA Journal,* Vol. 19, Feb. 1981, pp. 242-245.

[6] Küchemann, D., *The Aerodynamic Design of Aircraft,* Pergamon Press, London, 1978, Chap. 8.

[7] Pike, J., "Experimental Results from Three Cone-Flow Waveriders," AGARD Conference Proceedings No. 30, *Hypersonic Boundary Layers and Flow Fields,* London, May 1968.

[8] *Test Facilities Handbook,* 11th ed., "von Kármán Gas Dynamics Facility," Vol. 3, Arnold Engineering Development Center, Arnold Air Force Station, Tenn., June 1979.

[9] Lanham, D.L., "Static Force, Pressure, and Oil-Flow Visualization Tests of Supersonic Aerodynamic Lifting Bodies at Mach Numbers 3 to 5," AEDC TSR-80-V12, Arnold Engineering Development Center, Arnold Air Force Station, Tenn., Feb. 1980.